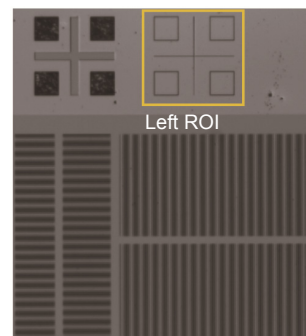# Plasmonic lithography with 100 nm overlay accuracy

Minggang Liu, Chengwei Zhao, Changtao Wang and Xiangang Luo*

State Key Laboratory of Optical Technologies on Nano-Fabrication and Micro-Engineering, Institute of Optics and Electronics, Chinese Academy of Sciences, Chengdu 610209, China

Left ROI

Abstract: In this paper, we demonstrate an auto accurate alignment method to align mask-substrate in the prototype of plasmonic lithography (PL), which is essential for multilayer nanostructure fabrication with high resolution, low cost, high efficiency, and high throughput, such as circuit manufacturing and other applications. We obtained an alignment signal with sensitivity better than 20 nm by using the Moiré fringe image. However, only using the Moiré fringes cannot guarantee the alignment of the mask and the substrate because the Moiré fringe repeats itself when the mask and substrate are offset by a fixed displacement. To eliminate the ambiguity, boxes and the crosses alignment marks are designed beside the grating marks on the substrate and the mask, respectively. A two-step alignment scheme including coarse alignment and fine alignment is explored in the auto alignment system. In the stage of coarse alignment, the edge detection algorithm based on Canny operator is adopted to detect the edges image effectively. In the process of fine alignment, Fourier transform based on Moiré fringe image is obtained to improve the alignment accuracy. In addition, experimental results of overlay indicate that PL can obtain sub-100 nm alignment accuracy over an area of 1 cm^2 using the proposed two-step alignment scheme. Via the substrate-mask mismatch compensation, better stages and precise environment control, it is expected that much higher overlay accuracy is feasible.

Keywords: Moiré fringe; surface plasmonic lithography; alignment

1 Introduction

The recent upsurge of research in surface plasmon (SP) rises in around 2000, which has provided a novel idea and practical approach to overcome the diffraction limit of optical lithography [1-2]. Compared with traditional optical lithography, SP lithography breaks through the optical resolution limit, and does not need complex lithography lens, expensive short wavelength light source and is compatible with the traditional optical devices [2-4]. With the gradual improvement of the lithography quality and resolution, SP lithography becomes an alternative technology of nano-optical fabrication with high resolution and low cost [5]. We present a lithography prototype by utilizing surface plasmons, as shown in Fig. 1. In the plasmonic lithography (PL) prototype, a plasmonic cavity lens composed of Ag-photoresist (PR)-Ag incorporating

high spatial frequency spectrum off-axis illumination is utilized to realize deep sub-wavelength imaging far beyond the near-field diffraction limit [6]. The prototype of PL offers a scheme of nano-fabrication with high resolution, low cost, and large area based on the stepper mode [7]. In fact, PL has found its way to applications in many disciplines where patterning of nanostructures is needed, such as sub-wavelength optics, single electron and quantum devices, molecular and bioelectronics, and nano- magnetic devices. But for multilayer structure manufacturing, isolated high resolution is insufficient, one must achieve high overlay alignment accuracy in addition to low defect density and high throughput.

The most important potential application of PL lies in integrated circuits (ICs). Automatic alignment acts as a key procedure to ensure that the substrate is exactly beneath the mask for precise pattern transform. The precise automatic alignment technology not only directly affects the overlay accuracy, but also influences the yield rate of PL. As a result, it is necessary to deploy accurate automatic alignment technology independent of operator's

skill for high precision and economic viability. Numerical solutions have been proposed to increase the alignment accuracy [8-9]. According to the operation principles, there are two typical alignment methods: video image alignment based on two geometric marks [10] and laser interference based on diffraction grating [11]. However, with the increasing demand of alignment accuracy, some disadvantages of the above methods appear. For example, video image technique depends highly upon extracting features of image, which results in a significantly limited alignment accuracy [12]. As for laser interference technique, the strict demand on the stability of complex system structure impedes its application in the prototype of PL. In order to overcome the disadvantages above, we proposed a Moiré fringe based on four sets gratings for the prototype of PL. The coarse-fine alignment method was also introduced. Furthermore, we conducted experiments involved both coarse and fine alignment to make it clear how the alignment scheme performs to achieve near perfect alignment performance.

2　Fundamental principle

Moiré fringes appear in the overlay of the repetitive structures and vary with the geometrical layout of the superposed structures. As shown in Fig. 2, two gratings G_1 and G_2, with respective period of P_1 and P_2 are superposed with tiny differences. The grooves of both gratings are aligned along the x or y axis. Diffractions take place on the surfaces of the two gratings successively when a planar wave normally incidents along the z axis. According to wave optics, any field can be regarded as a combination of the fields of all diffracted planar waves with different spatial frequencies. The optical field distribution [13] as $E(x, y, 0)$ can be simplified to be the following equation:

$$E(x,y,0) = \sum_{n=-\infty}^{+\infty} A_n \exp(\mathrm{j}\frac{2\pi}{\lambda}\sin\theta_n) =$$
$$\sum_{n=-\infty}^{+\infty} A_n \exp(\mathrm{j}\boldsymbol{k}_n x), \qquad (1)$$

where A_n and θ_n are the coefficient and diffractive angle of the nth diffractive order, respectively, λ is the wavelength of the incident light, and $\boldsymbol{k}_n = 2\pi n f_0$ is the transverse vector of the nth diffractive order, f_0 is the fundamental frequency of the grating. Similarly, the field behind two superposed gratings can also be regarded as a linear combination of fields of planar waves that diffract from these two gratings. Multi-diffractions usually occur at the surfaces of two superposed gratings to create a series of diffractive waves that overlap together and form certain irregular distribution. At the rear surface of G_1, the diffractive orders penetrate through the second grating G_2 and diffract again. The intensity distributions of these second diffraction waves are determined by the joint impacts of G_1 and G_2. Furthermore, when two linear gratings are used in alignment, the geometrical layout turns out to be denoted by linear functions. The diffracted wave that undergoes the mth diffraction at the first grating and the nth diffraction at the second grating is termed as the (m, n) order. For simplicity, the initial phases are neglected, and two symmetric orders are assumed to have the same amplitude under ideal conditions. The ultimate multi-diffractive orders jointly combine the optical field distributions as $E(x, y, 0)$, which can be simplified to the following expression [14]:

$$E(x,y,0) = \sum_{n=-\infty}^{+\infty}\sum_{m=-\infty}^{+\infty} A_n A_m \exp\{\mathrm{i}2\pi[(nf_1 + mf_2)\cdot x]\}, (2)$$

Here $E(x, y, 0)$ represents the transmission function, which is regarded as the field behind gratings when they are individually illuminated by a planar wave with unit amplitude, and f_1 and f_2 are the fundamental frequencies
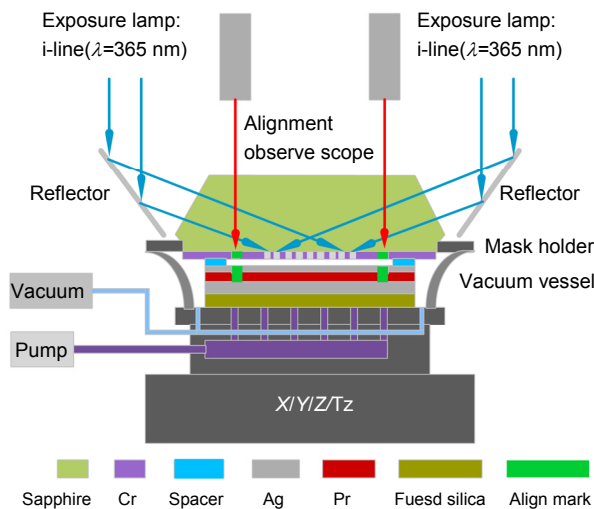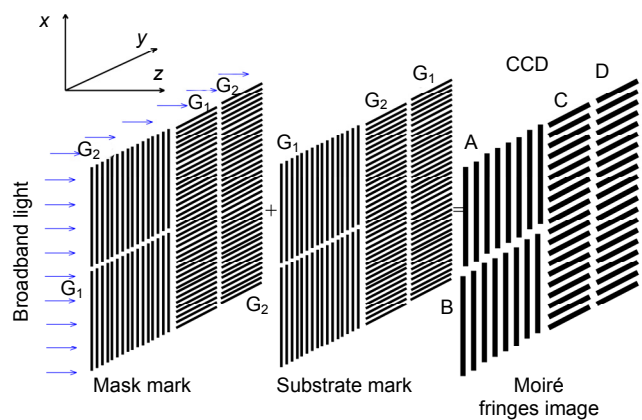

Fig. 1　Schematic diagram of PL prototype.

Fig. 2　Schematic of Moiré based substrate-mask alignment.

OEE | Advances

of G_1 and G_2. Considering a special case of Equation (2), $n = -m =1$ implies that the intensity distribution is just related to the period difference of the grating. The complex amplitude distribution of (1, -1) Moiré fringes produced by two superposed gratings that are transformed from two standard gratings with frequencies of f_1 and f_2 ($f_1 > f_2$) by the same transformation can be expressed as:

$$E(x,y,0) = \sum_{n=-1}^{+1} A_n B_{-n} \exp[i2\pi(f_1 - f_2) \cdot x].\quad (3)$$

Here only the orders of (1, 0) and (0, -1) participate the Moiré interferometry in our scheme. And the period of Moiré fringes can be easily expressed as: $P_{\text{Moire}} = P_1 P_2 / |P_1 - P_2|$. Obviously, the period of Moiré fringes is much larger than that of G_1 and G_2. Therefore, a tiny displaced shift between G_1 and G_2 can be illustrated by the obviously shift of Moiré fringes. This amplification can be used to detect a little relative position shift between the mask and substrate with accuracy in the nanometer range. By obtaining the phase difference between Moiré fringes pair of A and B, the misalignment in x direction can be written by:

$$\Delta x = \frac{\Delta \Phi_{\text{Moire}}}{2\pi} \left(\frac{P_1 P_2}{P_1 + P_2} \right),\quad (4)$$

where Δx is the alignment deviation of mask and substrate, $\Delta \Phi_{\text{Moire}}$ is the relative phase difference of two sets of Moiré fringes, P_1 and P_2 are the relative period of two sets of grating, respectively. The alignment in y direction is similar with the case of x direction. According to the interference and diffraction theory, Moiré fringe is independent of the illumination light wavelength and the length of the gap between the mask and the substrate, which make it very suitable for the prototype of PL.

3 Structure and operation of the alignment system

3.1 The structure of the alignment system

Fig. 3(a) shows the alignment schematic of the PL prototype. In the alignment system, a broadband light beam is passed through a grating mark on mask and reflected from the corresponding grating mark on the substrate and finally collected by objective lens and imaged onto CCD. As shown in Fig. 3(a), the alignment marks are the gratings with periods of $P_1 = 4.8$ μm and $P_2 = 4$ μm, forming a magnification factor of 6. To further improve Moiré fringe precision, we put both gratings G_1 and G_2 side by side on the sample and the complementary mark of G_2 and G_1 on the mask and substrate. When the substrate and the mask overlap, two sets of Moiré fringes of x direction and y direction move in opposite directions during the movement of the substrate relative to the mask, therefore, enhancing the magnification in overlay alignment accuracy by a factor of 2. Figs. 3(b) and 3(c) respectively illustrate the mask alignment mark and the substrate alignment mark. Both of them are composed of

linear grating arrays and "crosses" or "boxes". The substrate alignment mark has an inverse placement with that of the mask. Herein, the coarse alignment based on "crosses" and "boxes" leads the mask-substrate misalignment value into the range of fine alignment based on the Moiré fringes. There is a group of alignment marks on the left/right sides of the mask and substrate as shown in Figs. 3(d) and 3(e), respectively. And the length between the left and right alignment mark fields is 16.8 mm along the horizontal direction. Our alignment markers consist of three sets standard alignment "crosses", "boxes" structures and several grating patterns. Initially, the standard "cross" and "boxes" patterns are used for coarse alignment, which is used to overcome the ambiguity of the linear Moiré structures. Subsequently, high-precision alignment is achieved using the Moiré fringe signals. The two right and left-upper mask alignment marks have the same period P_1, while the remaining gratings have the same period P_2 ($P_1 > P_2$). The transverse grating pairs are used for the alignment in the x direction, and the longitudinal grating pairs are used for the alignment in the y direction.
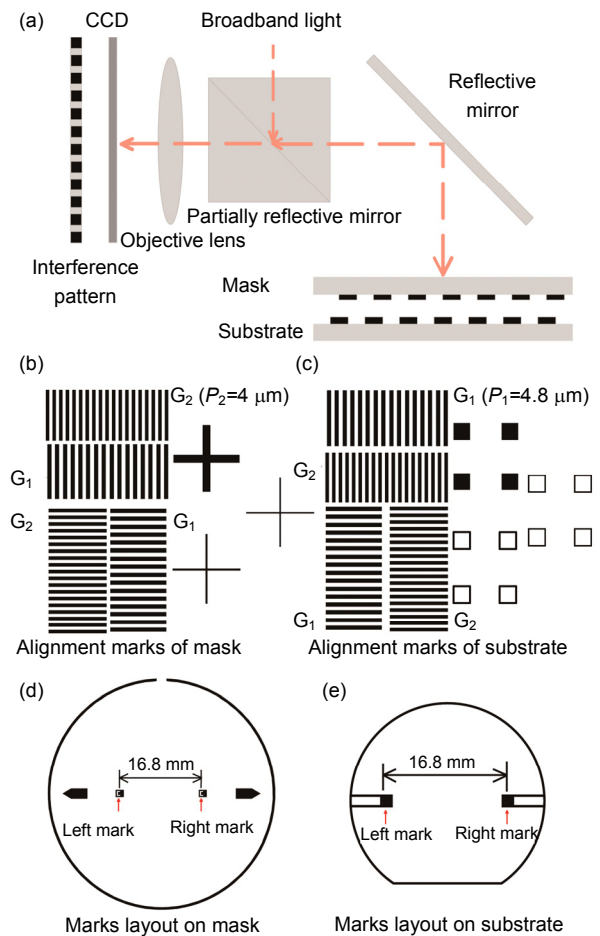

Fig. 3 (a) Schematic of alignment system in PL prototype. (b) The alignment marks of the mask. (c) The alignment marks of the substrate. (d) The alignment mark layouts on the mask. (e) The alignment mark layouts on the substrate.
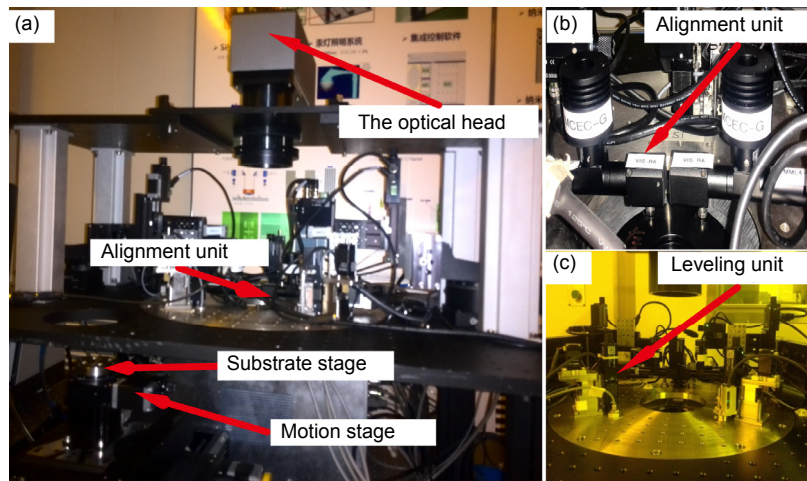
Fig. 4   Photograph of (a) whole system of our prototype, (b) the alignment unit and (c) the leveling unit.

3.2 Operation of the alignment system of PL

Fig. 4(a) shows the entire image of the prototype of PL. It consists of several parts, including an alignment illumination source, a diaphragm, a collimating lens, the mask alignment mark and the substrate alignment mark, a PI line stages translator (the resolution is respectively 50 nm (closed loop)), an imaging part and a computer, etc. An alignment illumination source, along with a collimating lens, provides a uniform and collimated light. The light beams illuminate onto the mask alignment mark and the substrate mark, where the Moiré fringes can be produced and collected through the CCD imaging system. The CCD (MVC300F) has 2048 pixels×1536 pixels. The magnification of the imaging lens is 8. The mask is mounted on a holder and the substrate is fixed on PI linear stage. PI linear stage is connected to a computer, which is used to control the relative displacement between the mask

and the substrate. The captured Moiré fringes patterns are processed using fast Fourier transform (FFT) to obtain the relative linear displacement. The system is carefully adjusted to achieve a uniform illumination and a clear Moiré fringe pattern on the CCD imaging system. The alignment marks on mask and substrate are adjusted to be parallel before alignment by a level mechanically through the proposed approach shown below, and the gap between the substrate and the mask is approximately within tens of micrometers.

4   Lithography experiment

4.1 Fabrication procedures for the substrate

The fabrication process of substrate with alignment marks is shown in Fig. 5(a). The fabrication started from the deposition of Cr film by magnetron sputtering (RF power 400 W, deposition rate 0.5 nm/s and temperature
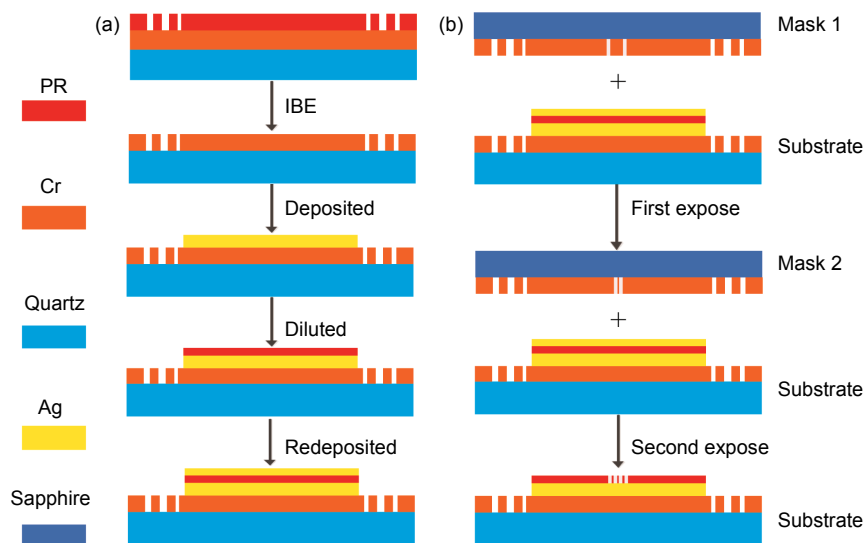

Fig. 5   (a) The schematic diagram of the fabrication of substrate. (b) The schematic diagram of the overlay experiment of PL.

300 °C) onto a fused silica substrate. The thickness of the deposited Cr film was 50 nm. Then, photoresist of AR-3170 (diluted by ALLRESIST GMBH, Strausbery, 30 nm @4000 rpm) was spin-coated on the top of Cr film and the substrate was planted in the prototype of PL as shown in Fig. 4. Subsequently, the alignment marks on the left and right sides were transferred into Cr film by wet etching. After that, the residual resist was removed by oxygen plasma etching with a power of 5 W and with O_2 flow of 10 sccm (stand cubic centimeter per minute) for 2 minutes. Afterwards, a layer of 50 nm thick Ag film was deposited on the central field of substrate via the thermal evaporation at a base pressure of 5.0×10^{-4} Pa with a deposition rate 5 nm/s. An approximate 30 nm thick PR of the diluted AR-3170 (diluted by ALLRESIST GMBH, Strausbery, 30 nm @ 4000 rpm) was spun onto the substrate to record the mask images. Finally, a 20-nm-thick Ag film was evaporated on the PR (base pressure of 5.0×10^{-4} Pa, deposition rate of 1 nm/s) after prebaking for 5 minutes on a hotplate at 100 °C.

4.2 Overlay procedures of PL prototype

The overlay process of the PL is shown in Fig. 5(b). First of all, the automatic alignment module aligns the substrate and mask 1 by using the alignment image from the left and right CCDs. Then the substrate is exposed performed by the first mask (Mask 1: four boxes) in the prototype of PL, as shown in Fig. 4. At this time, the first overlay alignment mark is transferred to the photo-resist. Afterwards, the same substrate is performed again by the second mask (Mask 2: cross mark) in the same manner. The plasmonic lithography was performed under the prototype of PL system, and applying air pressure (~0.1 MPa) to assure vacuum proximity. The SP was excited by a plane wave vertically impinging on the upside-down isosceles trapeze sapphire prism under a 365 nm mercury lamp illuminating system in the experiment. Finally, a physical method was used to peel off the top Ag film. After that, the substrate with photo-resist was developed by diluted AR 300-35 (ALLRESIST GMBH, Strausberg) with deionized water with the radio of 1:1 for 40 s at the temperature of 0 °C. Here, the overlay alignment marks of the first mask and the second mask were transferred to the same photo-resist layer.

4.3 The auto alignment procedures of PL

Figs. 6(a) and 6(b) show the optical images of four sets of Moiré fringe in the left alignment field and in the right alignment field, respectively. The experimental alignment results were captured by two MVC3000F CCDs with illumination of broadband light beams. For a perfect coarse alignment, the cross should be located at the center of the four boxes. During coarse alignment, CCD tracks the superposed patterns presented in Figs. 6(a) and 6(b). To detect the relative distance across mask-substrate "crosses" and "boxes" in the x direction, it is required that CCD can get the clear Moiré fringes image by

adjusting the linear stages. Then the extraction algorithm of region of interest (ROI) from image is used to get the zone that just include the "boxes" and "crosses" as shown in Figs. 6(c) and 6(d) to reduce the field size of image processing. Then we use the equalized algorithm and low pass filter algorithm to normalize the brightness and increase the contrast of the image. Next, we use the Canny algorithm and Gaussian smoothing algorithm to identify the edges of the capture image and return the marked image to alignment module. The rectangle identification module just only process the given rectangle including a range of 3600~6000 pixel² to avoid capture the irrelevant dirty that influences the accuracy and ratio of identification. Afterwards, the alignment module calculates the center of rectangle whose corner points are the center points of four given rectangles. The relative alignment accuracy is substituted by the difference between two center points of "boxes" and "crosses". Similarly, the misalignment in right alignment position can be calculated in the same way. Only when the theta is perfect should the x direction and y direction alignment be performed. When the misalignment is larger than 1 μm (predefined threshold deviation), PL auto alignment module keeps the mask motionless and drives sample stage to less deviation between mask and substrate until the deviation is less than we expected, which guarantees the misalignment across substrate and mask within the measurement range of fine alignment. Coarse alignment is finished when CCD image displays the cross mark is in the center of box marks, as shown in Figs. 6(c) and 6(d).
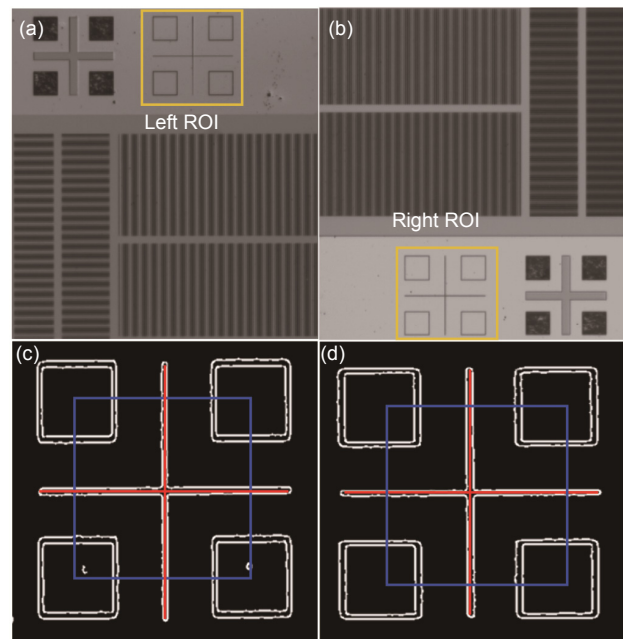

Fig. 6 (a) Optical image of alignment marks in the left alignment field. (b) Optical image of alignment marks in the right alignment field. (c) The coarse alignment mark image of left alignment field. (d) The coarse alignment mark image of right alignent field.

Followed by the coarse alignment shown in Figs. 6(c) and 6(d), the fine alignment based on the Moiré fringe image is further performed. Auto alignment module controls the CCD to capture alignment mark of Moiré fringe image generated by the overlaying two sets of gratings, as shown in Figs. 6(a) and 6(b). These captured alignment patterns are processed using FFT algorithm to obtain the alignment phase deviation. Then, auto alignment module calculates the x and y direction displacements and controls x-y stages to move until the left and right deviation of mask and substrate is less than the predefined threshold deviation. When it is satisfied, the substrate is brought closer to the mask. In this process, one should monitor the Moiré fringes carefully and adjust the position of the substrate when necessary. Because the vertical motion of the substrate toward the mask often results in lateral shift, fine alignment has to be adjusted carefully several times before the mask and substrate finally come into contact. After the alignment operation is completed, the phase relationship of the left alignment field between the two sets of Moiré fringes of x/y direction are shown in Figs. 7(a) and 7(b) and the phase relationship of the right alignment field are shown in Figs. 7(c) and 7(d). The red line indicates the phase value of the upper Moiré fringe, and the blue line indicates the phase value of the lower Moiré fringe, the phase difference between the two lines indicates that the mask and substrate are not completely aligned, and there is a sub-50 nm alignment deviation. It is seen from the phase diagram, with this method, we have achieved an accuracy of 50 nm for single point alignment for a 1 inch substrate.

5　Results and discussion

When mask aligns substrate perfectly, the cross should be at the center of the four boxes. In order to analyze the overlay accuracy, we tested the alignment accuracy at a single point. The overlay alignment accuracy was judged by SEM measurements of the alignment of the cross and the box marks as shown in Figs. 8(a) and 8(b). An overlay error was calculated by the difference between two center points of "boxes" and "crosses". To evaluate the alignment method, nine points in the area up to 1 cm² of substrate were measured relative to underlying pattern to decide an overlay accuracy of the substrate in the x and y directions. The alignment error on a point was defined: $(\Delta x^2 + \Delta y^2)^{1/2}$. As shown in Fig. 8(c), the blue, red and green lines denote the alignment error in x direction, y direction and single point alignment, respectively. From Fig. 8(c), we can see that the standard deviation of the misalignment is below 20 nm in both x and y directions. The overlay alignment errors vary from point to point in a random manner, which come mainly from several factors, such as the errors in layout the patterns on the masks and on the substrate, our stage accuracy, the distortion caused by the variation of stress on the substrate, and local temperature variation on the substrate. The advantages of the implemented Moiré technique are the relative simplicity of the design. Furthermore, the whole setup combined with the possibility of an unproblematic upgrade of the prototype of PL still provides ultra-high precision alignment capabilities. Clearly, the precision overlay alignment method greatly expands the application scope of PL.
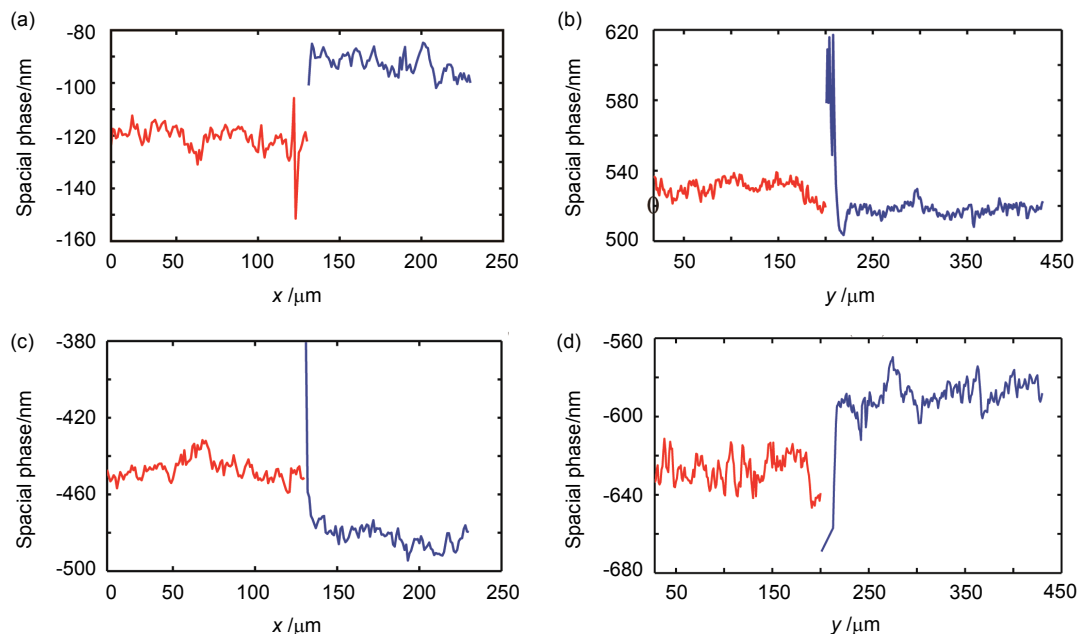

Fig. 7　(a) Spatial phase as a function of x location of left alignment field. (b) Spatial phase as a function of y location of left alignment field. (c) Spatial phase as a function of x location of right alignment field. (d) Spatial phase as a function of y location of right alignment field.
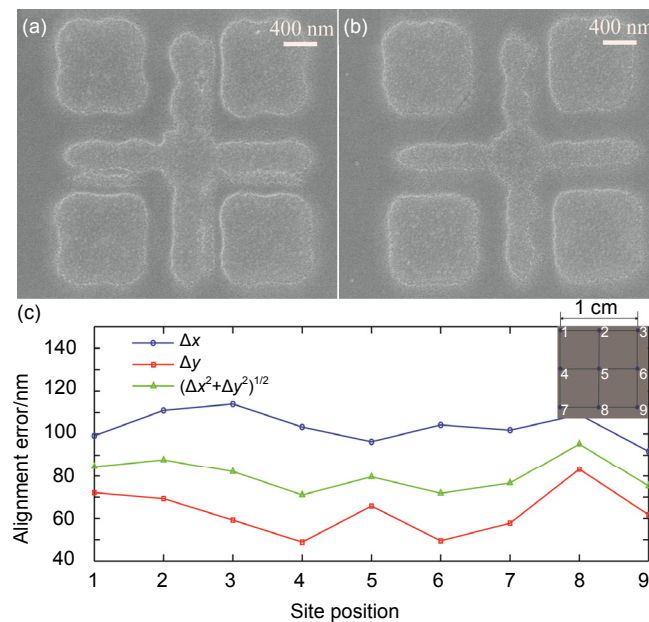
Fig. 8 (a) SEM image of two sets of overlay marks in the first site position (four boxes for the first mask and a cross for the second mask). (b) SEM image of two sets of overlay marks in the last site position. (c) Statistics of misalignment with 9 measurement sites on 1 cm^2 on 1 in substrate.

6   Conclusions

In this work, we have demonstrated a high-precision alignment approach based on Moiré fringes for the prototype of PL. The alignment signal remains measureable throughout and after the whole lithography process, and does not depend on the gap between the mask and the substrate. The experimental results indicate that we have achieved an accuracy of sub-100 nm overlay accuracy for a full 1 inch substrate by the cooperation of coarse alignment and fine alignment operation. Furthermore, the auto alignment system and its process are also fully scalable for 4 inch or larger substrate processing. It is believed that the prototype of PL with auto alignment scheme, as a low cost, high resolution and large area fabrication process, would find potential applications in the fabrication of multilayer nanostructures.

Acknowledgements

References

1   Pendry J B. Negative refraction makes a perfect lens[J]. *Physical Review Letters*, 2000, **85**(18): 3966–3969.

2   Luo Xiangang, Ishihara T. Surface plasmon resonant interference nanolithography technique[J]. *Applied Physics Letters*, 2004, **84**(23): 4780–4782.

3   Fang Nicholas, Lee Hyesog, Sun Cheng, *et al*. Sub-diffraction-limited optical imaging with a silver superlens[J]. *Science*, 2005,

308: 534–537.

4   Holzwarth C W, Foulkes J E, Blaikie R J. Increased process latitude in absorbance-modulated lithography via a plasmonic reflector[J]. *Optics Express*, 2011, **19**(18): 17790–17798.

5   Luo Jun, Zeng Bo, Wang Changtao, *et al*. Fabrication of anisotropically arrayed nano-slots metasurfaces using reflective plasmonic lithography[J]. *Nanoscale*, 2015, **7**: 18805– 18812.

6   Zhao Zeyu, Luo Yunfei, Zhang Wei, *et al*. Going far beyond the near-field diffraction limit via plasmonic cavity lens with high spatial frequency spectrum off-axis illumination[J]. *Scientific Reports*, 2015, **5**: 15320.

7   Liu Minggang, Zhao Chengwei, Luo Yunfei, *et al*. Subdiffraction plasmonic lens lithography prototype in stepper mode[J]. *Journal of Vacuum Science & Technology B*, 2017, **35**(1): 011603–011611.

8   Chen Wangfu, Yan Wei, Hu Song, *et al*. Extended dual-grating alignment method for optical projection lithography[J]. *Applied Optics*, 2010, **49**(4): 708–721.

9   Li N, Wu W, Chou S Y. Sub-20-nm alginemnt in nanoimprint lithography using morie fringes[J]. *Nano Letters*, 2006, **6**(11): 2626–2629.

10   Nishi K. Method of aligning a substrate: US Patent, 5,682.243 [P]. 1997.

11   Kinoshita H, Une A, Iki M. A dual grating alignment technique for X-ray lithography[J]. *Journal of Vacuum Science & Technology B*, 1983, **1**(4): 1276–1279.

12   Di Chengliang, Zhu Jiangping, Yan Wei, *et al*. A modified alignment method based on four-quadrant-grating Moiré for proximity lithography[J]. *OPTIK*, 2014, **124**(17): 4868–4872.

13   Goodman J W. Introduction to fourier optics, second edition [J]. *Optical Engineering*, 1996, **35**(5): 1513–1518.

14   Bryngdahl. Moire: Formation and interpretation[J]. *Journal of the Optical Society of America*, 1974, **64**(10): 1287–1294.